

Single-site orthogonalization for first-principles computations of exchange coupling constants

Asako Terasawa,^{1,*} Sonju Kou,¹ Taisuke Ozaki,² and Yoshihiro Gohda^{1,†}

¹*Department of Materials Science and Engineering, Tokyo Institute of Technology, J1-3, Nagatsuta-cho 4259, Midori-ku, Yokohama 226-8502, Japan*

²*Institute for Solid State Physics, The University of Tokyo, Kashiwanoha 5-1-5, Kashiwa 277-8581, Japan*

For accurate first-principles computations of exchange coupling constants J_{ij} by the Liechtenstein method with localized basis sets, we developed a scheme using the single-site orthogonalization (SO). In contrast to the non-orthogonal (NO) scheme, where the basis set is used to compute J_{ij} without modification, and the Löwdin orthogonalization (LO) scheme, the SO scheme exhibits much less dependence of J_{ij} on the choice of the basis set. The SO scheme achieves convergence of J_{ij} for bcc Fe, hcp Co, and fcc Ni with an increase in the number of the basis set, while the NO and LO schemes result in the fluctuation depending on the basis set. This improvement by the SO scheme is attributed to the removal of orbital overlaps with avoiding ill-defined single-site effective potentials. We further improve the SO scheme by introducing appropriate spin population, so that the SO with spin-population scaling (SOS) scheme can provide converged Curie temperatures for transition metals. Moreover, negative values of J_{ij} for dhcp Nd and rhombohedral Sm obtained by the SOS scheme can coincide with the experimentally-found magnetic order that cannot be reproduced by positive sets of J_{ij} .

I. INTRODUCTION

Improving the performance of permanent magnets is one of the most pressing technological requirements from industry for achieving high energy-efficient society. The key to this lies in understanding the microstructures of permanent magnets, because the microstructure properties determine the movement of the internal magnetic domain walls [1–8]. The structural complexities of permanent magnets, however, often prevents us from reaching a simple understanding of their magnetic properties. For example, crystallinity and compositions of grain boundary phases vary depending on their local environments [9, 10].

Recently, first-principles calculation techniques have been employed to investigate the magnetic properties of permanent magnets [11–25]. Because of the multiple phases and types of internal interfaces in permanent magnets, many problems remain unsolved. In particular, the exchange couplings between the various phases are important in achieving high-performance permanent magnets [7].

The idea of extracting the exchange coupling constants from ground state calculations was first established by Oguchi *et al.* [26] and further developed by Liechtenstein *et al.* [27]. The magnetic force theorem, also known as the Liechtenstein method, is a powerful tool for computing of the exchange coupling constants in the classical Heisenberg model. The Hamiltonian of the classical Heisenberg model can be written as in the following equation:

$$E = - \sum_i \sum_{j \neq i} J_{ij} \mathbf{s}_i \cdot \mathbf{s}_j, \quad (1)$$

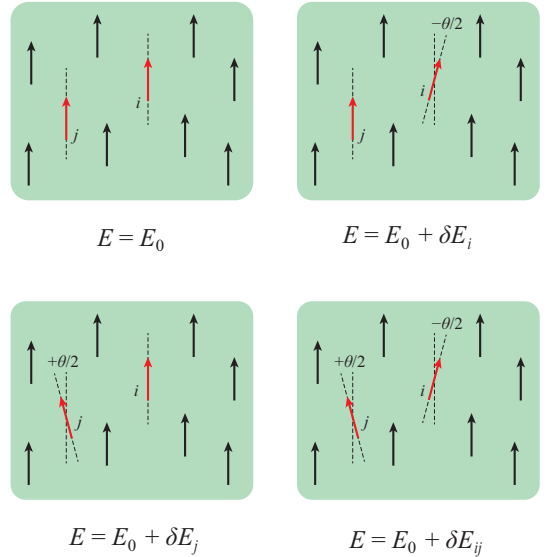


FIG. 1. A schematic of infinitesimal spin rotations in Liechtenstein method.

where \mathbf{s}_i is the unit vector along the spin direction of site i . In the Liechtenstein method, one aims to extract the exchange coupling constant J_{ij} by calculating the difference in energy response to infinitesimal rotations of effective potential at sites i and j shown schematically in Fig. 1:

$$\delta' E_{ij} \equiv \delta E_{ij} - \delta E_i - \delta E_j = J_{ij} \frac{\theta^2}{2}. \quad (2)$$

Making use of the second perturbation theory, the exchange coupling constant can be written as

$$J_{ij} = \frac{1}{4\pi} \int d\varepsilon f_F(\varepsilon) \text{ImTr} \left[\hat{P}_i \hat{G}_\uparrow(\varepsilon) \hat{P}_j \hat{G}_\downarrow(\varepsilon) \right], \quad (3)$$

* terasawa.a.aa@m.titech.ac.jp

† gohda.y.ab@m.titech.ac.jp

where $\hat{G}_\sigma(\varepsilon)$ is the retarded Green's function of the spin σ for collinear states, and

$$\hat{P}_i \equiv \hat{V}_{i,\uparrow} - \hat{V}_{i,\downarrow}$$

is the difference in electronic potential at site i .

Since its establishment, there have been many works on improving Liechtenstein methods within the KKR Green's function formalism [28–33], and applying the Liechtenstein method to other electronic calculation schemes, such as the linear muffin-tin orbital method [34–39] and the linear combination of atomic orbitals (LCAO) approximation [40–42]. A cumbersome problem arises here: the exchange coupling constants in the previous studies often fluctuate on the order of meV, which results in fluctuations of a few hundred Kelvins in the Curie temperature [34, 35, 37, 38, 41, 42]. The dependence of the J_{ij} fluctuation on the computational scheme has been examined by Kvashnin *et al.* [38]. They compared the J_{ij} calculated with two definitions of basis functions for single atomic sites, namely a simple integration cutoff outside the radius of the muffin-tin potential was adopted in one definition, and Löwdin orthogonalized (LO) overlapping basis functions in the other definition. They found a deviation between the J_{ij} calculated with the two definitions, and suggested that the deviation originated from the deviation in the single-site electron populations in the two definitions. Their conclusion highlights the difficulty in determining well-defined values of J_{ij} , especially in the presence of overlap of atomic orbitals. This problem is also related to the problem of itinerancy, because wide-ranged basis functions are necessary to represent itinerant states accurately.

In this paper, we report a new scheme for calculating the exchange coupling constants in first-principles calculations within the LCAO approximation. We examine the calculated J_{ij} values of bcc Fe for different choices of basis sets in detail. We find that the matrix representation of the Hamiltonian using non-orthogonal (NO) atomic orbitals is unsuitable for representing the single-site potential in the presence of large overlap, and that the computational results vary with the choice of basis set. To solve this problem, we introduce a single-site orthogonalization (SO) scheme for representing an effective single-site potential within the LCAO approximation. The calculated J_{ij} values decrease slightly with increasing numbers of basis functions, while the results from the NO and LO schemes fluctuate significantly with the number of basis functions. To overcome the slight decrease in J_{ij} , we introduce a spin population scaling in the SO scheme, namely the single-site orthogonalization with spin-population scaling (SOS). Using the SOS scheme, we successfully obtain converged J_{ij} curves as functions of the atomic distance r_{ij} when the number of basis functions is increased. We also apply the SOS scheme to calculate the J_{ij} of various systems and their transition temperatures within the mean field approximation. It is then possible to obtain converged Curie temperatures for bcc Fe, hcp Co and fcc Ni. For dhcp Nd and rhombohedral Sm, we obtained weak negative

J_{ij} curves. Our results corresponds to the experimental reports of spiral and complicated magnetic orders of Nd and Sm [47] indicating antiferromagnetic exchange couplings.

II. SINGLE-SITE POTENTIAL AND ORTHOGONALIZATION SCHEME

To formulate the Liechtenstein method within the LCAO approximation, it is necessary to first define the single-site potential in the presence of overlap of atomic orbitals. The simplest approximation is just to apply i - and j -th diagonal elements of the total Hamiltonian:

$$P_{ii} \equiv H_{ii,\uparrow} - H_{ii,\downarrow}, \quad (4)$$

$$H_{ij,\sigma} \equiv \langle i | \hat{H}_\sigma | j \rangle \quad (5)$$

to generate the single-site potential operator, where $|i\rangle$ and $|j\rangle$ represent the non-orthogonal atomic orbitals for the sites i and j . For simplicity, we assume here a single orbital for each atomic site. The corresponding operator notation of i -th single-site potential for the above approximation can be written as

$$\hat{P}_i^{(\text{NO})} \equiv \sum_{j,j'} |j\rangle [\mathbf{S}^{-1}]_{ji} P_{ii} [\mathbf{S}^{-1}]_{ij'} \langle j'|, \quad (6)$$

where the notation (NO) represents that the operator is generated straightforwardly from the matrix representation by non-orthogonal atomic orbitals. For the definition (6), it is necessary to define the overlap matrix \mathbf{S} for non-orthogonal basis set $\{|j\rangle\}$:

$$\langle i | j \rangle = 1 \quad (7)$$

$$\langle i | j \rangle = [\mathbf{S}]_{ij} \quad (i \neq j), \quad (8)$$

where $[\mathbf{A}]_{ij}$ means the (i, j) element of matrix \mathbf{A} .

The physical meaning of $\hat{P}_i^{(\text{NO})}$ is however ambiguous in the presence of large overlap of atomic orbitals belonging to different sites. When the off-diagonal elements of \mathbf{S}^{-1} are large, many orbitals corresponding to other sites are involved into Eq. (6), and $\hat{P}_i^{(\text{NO})}$ is no longer single-site like.

To avoid the problem of ambiguity caused by overlap of atomic orbitals, orthogonalization schemes are often adopted. One of the most straightforward orthogonalization schemes is Löwdin orthogonalization (LO):

$$|\tilde{i}\rangle \equiv \sum_j |j\rangle [\mathbf{S}^{-1/2}]_{ji}. \quad (9)$$

We can easily prove that the Löwdin orbitals belonging to different sites are orthogonal to one another. With the LO basis set, we define the effective single-site potential by LO scheme as:

$$\hat{P}_i^{(\text{LO})} \equiv |\tilde{i}\rangle P_{ii}^{(\text{LO})} \langle \tilde{i}| \quad (10)$$

$$P_{ii}^{(\text{LO})} \equiv \langle \tilde{i} | \hat{H}_\uparrow | \tilde{i} \rangle - \langle \tilde{i} | \hat{H}_\downarrow | \tilde{i} \rangle. \quad (11)$$

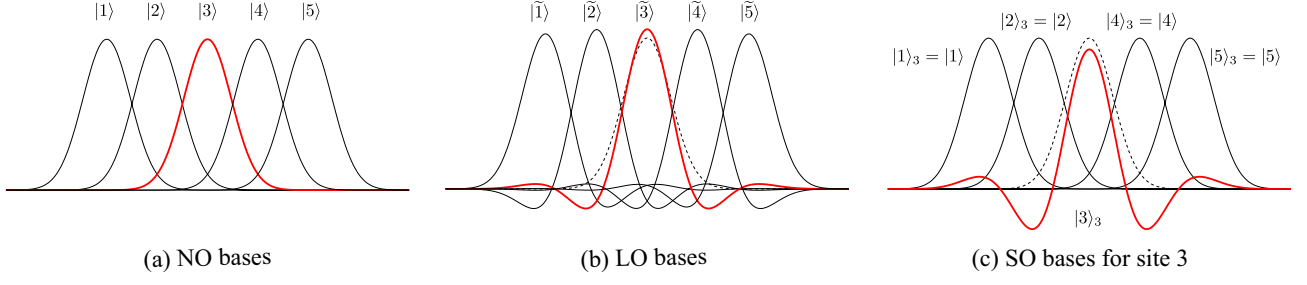


FIG. 2. A non-orthogonal basis set and its corresponding orthogonalized basis sets, described by one-dimensional Gaussian functions and their linear combinations. In each panel, the red solid line represents the basis belonging to site 3, and black solid lines represent the basis functions belonging to other sites. In panels (b) and (c), the dotted black line represents the original NO basis at site 3. (Color online)

In addition to the LO basis set, we also consider single-site orthogonalized (SO) orbitals in this study. In the SO scheme, the orbital belonging to a particular site in the basis set is made orthogonal to other orbitals, whereas other pairs of atomic orbitals remain unchanged. To define the SO bases for site i , we first define the neighbor set \bar{i} for site i as:

$$\bar{i} \equiv \{j \mid j \neq i, \langle i|j\rangle \neq 0\}. \quad (12)$$

In other words, the neighbor set \bar{i} of site i is defined as the set of sites that has nonzero overlap with site i , but excludes site i itself. It is then possible to define the partial overlap matrix $\mathbf{S}_{\bar{i},i}$ between the site i and the sites in the neighbor set \bar{i} as

$$[\mathbf{S}_{\bar{i},i}]_{ji} \equiv \langle j|i\rangle, j \in \bar{i} \quad (13)$$

and the partial overlap matrix $\mathbf{S}_{i,\bar{i}}$ between sites in the neighbor set \bar{i} as

$$[\mathbf{S}_{i,\bar{i}}]_{jj'} \equiv \langle j|j'\rangle, j, j' \in \bar{i}. \quad (14)$$

Here, the matrix $\mathbf{S}_{i,\bar{i}}$ has a dimension of $N(\bar{i}) \times 1$ and the matrix $\mathbf{S}_{\bar{i},i}$ has a dimension of $N(\bar{i}) \times N(\bar{i})$, where $N(\bar{i})$ is the number of neighboring sites to site i . Given the partial matrices $\mathbf{S}_{\bar{i},i}$ and $\mathbf{S}_{i,\bar{i}}$, the SO bases that isolates site i are

$$|i\rangle_i \equiv |i\rangle - \sum_{j \in \bar{i}} |j\rangle [\mathbf{S}_{\bar{i},i}^{-1} \mathbf{S}_{i,\bar{i}}]_{ji} \quad (15)$$

$$|j\rangle_i \equiv |j\rangle, j \neq i. \quad (16)$$

From the definitions, we can easily prove that

$$\langle i|i\rangle_i = 0, j \neq i,$$

while any other combinations of SO bases are left non-orthogonal.

For a simple example, we examine a five-site system with NO bases described by one-dimensional Gaussian functions as shown in Fig. 2(a), and the corresponding LO and SO basis functions as shown in Figs. 2(b) and (c), respectively. It can be seen that the LO basis functions

have similar structures to the NO basis functions around their maxima and small damped oscillations at their tails. In contrast, the SO basis functions oscillate more prominently around their respective sites of focus, as shown in Fig. 2(c). This oscillation cancels the overlaps with the other orbitals which are left unchanged from the original NO bases.

Defining the SO basis set, it is possible to define the effective single-site potential as

$$\begin{aligned} \hat{P}_i^{(\text{SO})} &\equiv |i\rangle_i \mathbf{S}_{ii}^{-1} \\ &\times \left(\langle i|\hat{H}_\uparrow|i\rangle_i - \langle i|\hat{H}_\downarrow|i\rangle_i \right) \\ &\times \mathbf{S}_{ii}^{-1} \langle i|_i \end{aligned} \quad (17)$$

$$\mathcal{S}_{ii} \equiv \langle i|i\rangle_i = 1 - \mathbf{S}_{i,\bar{i}} \mathbf{S}_{\bar{i},i}^{-1} \mathbf{S}_{i,\bar{i}}. \quad (18)$$

Applying the above definition to Eq. (3), we obtain the exchange coupling constant based on the SO basis as

$$\begin{aligned} J_{ij}^{(\text{SO})} &= \frac{1}{4\pi} \int_{-\infty}^{\infty} d\varepsilon f(\beta(\varepsilon - \varepsilon_F)) \\ &\times \text{Im} \left\{ P_{ii}^{(\text{SO})} G_{ij,\uparrow}(\varepsilon) P_{jj}^{(\text{SO})} G_{ji,\downarrow}(\varepsilon) \right\}, \end{aligned} \quad (19)$$

$$\begin{aligned} P_{ii}^{(\text{SO})} &\equiv \langle i|\hat{P}_i^{(\text{SO})}|i\rangle = \langle i|\hat{H}_\uparrow|i\rangle_i - \langle i|\hat{H}_\downarrow|i\rangle_i \\ &= P_{ii} - \mathbf{P}_{i,\bar{i}} \mathbf{S}_{\bar{i},i}^{-1} \mathbf{S}_{i,\bar{i}} - \mathbf{S}_{i,\bar{i}} \mathbf{S}_{\bar{i},i}^{-1} \mathbf{P}_{\bar{i},i} \\ &\quad + \mathbf{S}_{i,\bar{i}} \mathbf{S}_{\bar{i},i}^{-1} \mathbf{P}_{\bar{i},i} \mathbf{S}_{\bar{i},i}^{-1} \mathbf{S}_{i,\bar{i}}, \end{aligned} \quad (20)$$

where

$$[\mathbf{P}_{i,\bar{i}}]_{ji} \equiv H_{ji,\uparrow} - H_{ji,\downarrow}, j \in \bar{i} \quad (21)$$

$$[\mathbf{P}_{\bar{i},i}]_{jj'} \equiv H_{jj',\uparrow} - H_{jj',\downarrow}, j, j' \in \bar{i} \quad (22)$$

$$G_{ij,\uparrow}(\varepsilon) \equiv \sum_n \frac{C_{i,n\uparrow} C_{j,n\uparrow}^*}{\varepsilon + i\eta - \varepsilon_{n\uparrow}} \quad (23)$$

$$G_{ji,\downarrow}(\varepsilon) \equiv \sum_n \frac{C_{j,n'\downarrow} C_{i,n'\downarrow}^*}{\varepsilon + i\eta - \varepsilon_{n'\downarrow}}, \quad (24)$$

and $\varepsilon_{n\sigma}$ and $\mathbf{C}_{n\uparrow}$ are the eigenvalues and eigenvectors of the LCAO Hamiltonian.

We can also expand the definitions of LO and SO bases to periodic systems with multi-orbital atoms. For such

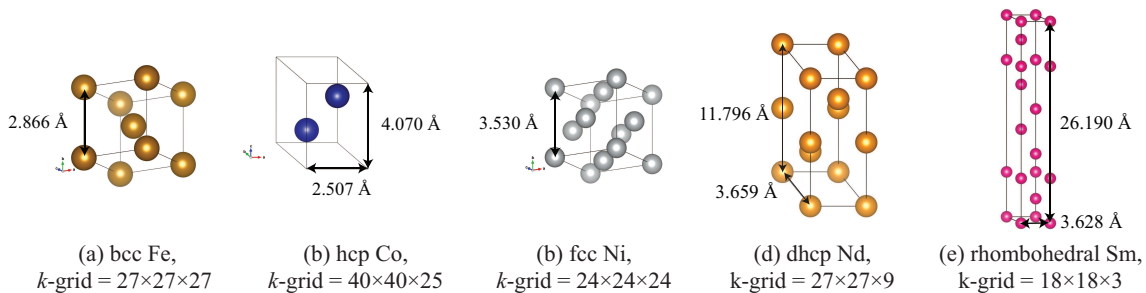


FIG. 3. Computational models of unit cells for transition metals and rare earth metals examined in this study. The notation k -grid = $a \times b \times c$ in each figure corresponds to the number of reciprocal space grids in first-principles calculations. (Color online)

systems, the LO bases are written as

$$|\widetilde{\mathbf{R}}, i, \mu\rangle \equiv \sum_{\mathbf{k}} \sum_{j, \nu'} |\mathbf{k}, j, \nu'\rangle [\mathbf{S}^{-1/2}]_{\mathbf{k}j\nu', \mathbf{R}i\mu} e^{-i\mathbf{k} \cdot \mathbf{R}/2}, \quad (25)$$

and the SO bases are written as

$$|\mathbf{R}, i, \mu\rangle_{\mathbf{R}, i} \equiv |\mathbf{R}, i, \mu\rangle - \sum_{\mathbf{R}' \in \overline{\mathbf{R}i}} \sum_{\nu} |\mathbf{R}', j, \nu\rangle \times [\mathbf{S}_{\overline{\mathbf{R}i}, \overline{\mathbf{R}i}}^{-1} \mathbf{S}_{\overline{\mathbf{R}i}, \mathbf{R}i}]_{\mathbf{R}'j\nu, \mathbf{R}i\mu} \quad (26)$$

$$|\mathbf{R}', j, \nu\rangle_{\mathbf{R}, i} \equiv |\mathbf{R}', j, \nu\rangle, (\mathbf{R}', j) \neq (\mathbf{R}, i). \quad (27)$$

Here, $|\mathbf{R}, i, \mu\rangle$ is the μ -th atomic orbital belonging to atom i of cell \mathbf{R} , and $|\mathbf{k}, i, \mu\rangle$ is the Bloch orbital corresponding to the atomic orbitals of atom i . In Sec. IV, we compare the J_{ij} values calculated by the three schemes for various systems.

III. COMPUTATIONAL MODELS AND METHODS

Figure 3 shows the computational models examined in this study, namely (a) bcc Fe, (b) hcp Co, (c) fcc Ni, (d) dhcp Nd, and (e) rhombohedral Sm. The numbers of reciprocal space grid points are determined dependent on the systems sizes, and they are three as k -grid = $a \times b \times c$ in Fig. 3.

For the first-principles calculations based on the LCPAO approximation, we performed the density functional calculations using the OpenMX code [43] (Here PAO in LCPAO means pseudo atomic orbitals, which are basically the same as atomic orbitals except for the exact finite cutoffs). For the exchange correlation functional, we adopted the Perdew-Burke-Ernzerhof exchange-correlation functional [44] within the generalized gradient approximation (GGA-PBE). For the pseudo atomic orbitals, the cutoff radii were set to 6.0 Bohr for Fe, Co, and Ni, and to 10 Bohr for Sm and Nd.

In the spin-dependent SCF calculations, we assumed ferromagnetic configuration of the spin populations for all the systems examined. We used an electronic temperature of 300 K, and the convergence criterion for the total energy was set as 1.0×10^{-6} Ha.

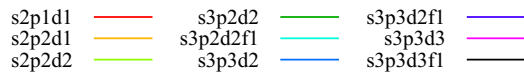
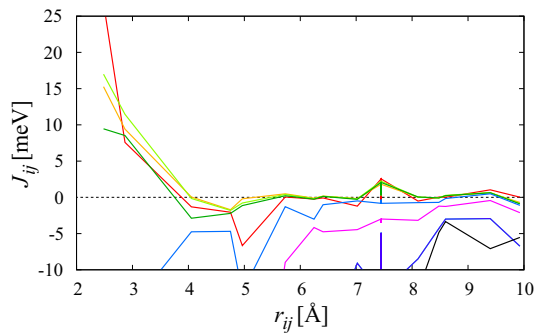
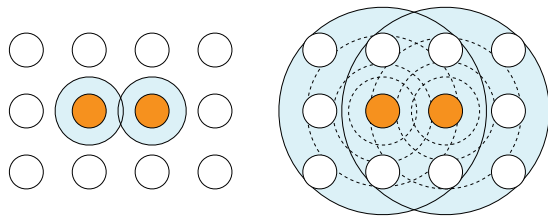
Our implementation of the Liechtenstein formula was based on the finite pole approximation of the Fermi function [45] in which the energy integration over the real axis in Eq. (3) was substituted by summation over a finite number of poles of the approximated Fermi function. The implementation is reported in detail in Ref. [42].

To examine overlap effects, different choices of basis sets were examined in this paper. The minimal basis sets were constructed from $3s$, $3p$, $3d$, and $4s$ orbitals for Fe, Co, and Ni atoms, and from $5s$, $5p$, $5d$, and $6s$ orbitals for Nd and Sm atoms. The $4f$ states of Nd and Sm were treated as spin polarized core states. When extensive basis sets were adopted, we included orbitals having more spreading basis distributions, which resulted in larger overlaps between different sites. To describe the effect of the core states, we adopted the fully relativistic pseudopotentials generated by the Morrison-Bylander-Kleinman scheme [46].

IV. RESULTS

A. Detailed Analysis of J_{ij} for bcc Fe

We first present the exchange coupling constants J_{ij} of bcc Fe in Fig. 4(a) as functions of atomic distances r_{ij} for the NO scheme. In Fig 4(a), the lines of different colors correspond to different choices of basis sets from s2p1d1 to s3p3d3f1. Here, the notation $sxpydzfw$ means that the basis set is constructed from x types of s orbitals, y types of p orbitals, z types of d orbitals, and w types of f orbitals. The total number of basis functions N_b per atomic site is thus $(x + 3y + 5z + 7w)$ for the notation $sxpydzfw$. A remarkable feature can be seen in Fig. 4(a) where the J_{ij} profiles are similar for s2p2d1, s2p2d2, and s3p2d2 with fluctuations of about a few meV, whereas the J_{ij} profiles deviate strongly to negative values for the larger basis sets.

(a) J_{ij} of bcc Fe by NO scheme

(b) Schematic of orbitals for minimal basis set

(c) Schematic of orbitals for extensive basis set

FIG. 4. (a) Exchange coupling constants J_{ij} as functions of atomic distance r_{ij} for the NO scheme and different choices of basis sets. (b) and (c) Schematics of orbitals for different choices of basis sets. (Color online)

This feature seems strange at first sight because the calculations of the electronic states themselves become more accurate as we increase the total number of basis functions. To understand the feature, it is necessary to consider the relationship between the single-site potentials and the LCAO Hamiltonian matrix elements. Figures 4(b) and (c) show the relationships between the orbitals and atomic sites schematically. When we choose the minimal basis set, we only take into account combinations of orbitals which have small ranges as shown in Fig. 4(b). In this case, the electronic potentials in the considered ranges can be regarded as effective single-site potentials, and thus the Liechtenstein formula works well. When we choose an extensive basis set, in contrast, more spreading basis functions for each site are taken into account in the calculation as shown in Fig. 4(c). In this case, the range of a single orbital spans multiple atoms, and the matrix elements for wide orbitals are no longer effective single-site potentials. This results in the breakdown of the Liechtenstein formula when adopting non-orthogonal Hamiltonian for effective potential terms. While the instability at large N_b becomes natural with this reasoning, the instability results in a cumbersome problem: we cannot determine accurate J_{ij} values simply by adopting NO Hamiltonians as effective single-site potentials from the LCAO calculation.

In order to stabilize the calculation results for differ-

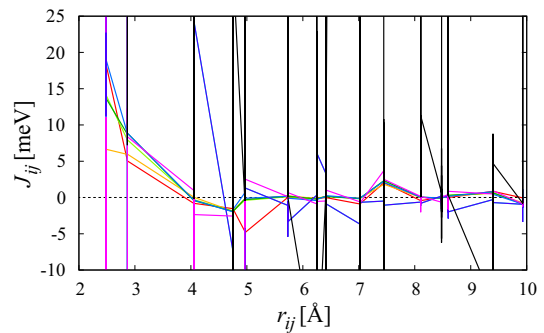
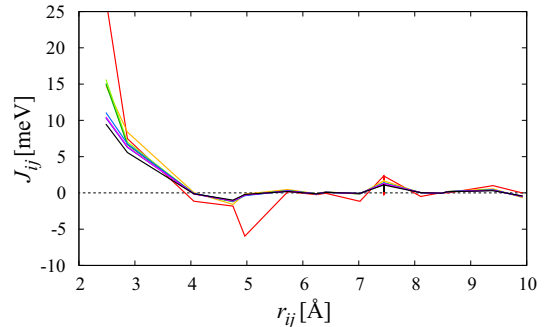
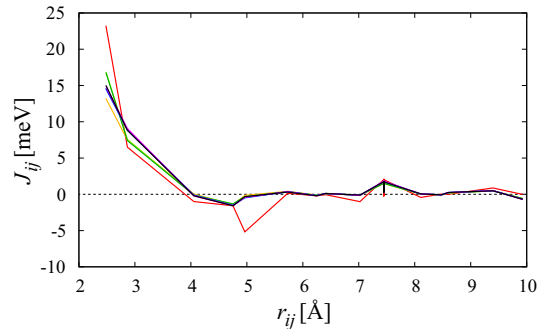
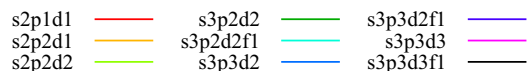
(a) J_{ij} of bcc Fe by LO scheme(b) J_{ij} of bcc Fe by SO scheme(c) J_{ij} of bcc Fe by SOS scheme

FIG. 5. Exchange coupling constants J_{ij} of bcc Fe as functions of atomic distances r_{ij} for different orthogonalization schemes and choices of basis sets. (Color online)

ent choices of basis sets, we examined the two types of orthogonalization schemes which have been explained in the previous sections, namely the LO and SO schemes, as shown in Figs. 5(a) and (b). It is apparent that the LO scheme does not solve the problem illustrated in Fig. 5(a). The calculated J_{ij} values do not converge either, and fluctuate strongly for large N_b . This indicates that the LO scheme fails to represent effective single-site potentials in the presence of overlapped atomic orbitals. That is, an electron described by an LO function at a specific atomic site feels the potential coming from other atoms, and thus the diagonal elements of the Hamiltonian in the

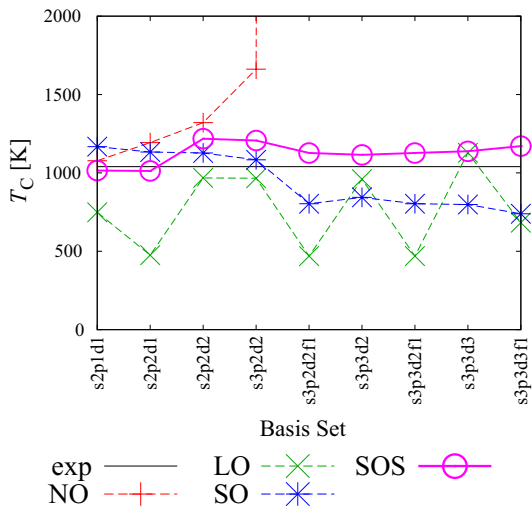


FIG. 6. Calculated Curie temperatures of bcc Fe within mean field approximation for different orthogonalization scheme and different choices of basis sets, together with the experimental values. (Color online)

LO representation include the contributions of multiple atoms.

In contrast, the J_{ij} results calculated with the SO scheme show a relatively stable behavior but decrease slightly with increasing N_b . The stability of the J_{ij} curves in the SO scheme indicates that the overlap cancellation by damped oscillations also works well for the matrix representation of the Hamiltonian, and that the single-site Hamiltonian is well described by the SO scheme.

The gradual decrease of J_{ij} in the SO scheme is however non-negligible. This may have resulted from the deviation of the spin population depending on the choice of basis set, as pointed out in Ref. [38]. In particular, the SO scheme tends to underestimate the spin population, because it subtracts the components of other atoms from the basis of the focused site. To eliminate the underestimation, we introduce spin population scaling as follows:

$$J_{ij}^{(\text{SOS})} \equiv \frac{\Delta n_i}{\Delta n_i^{(\text{SO})}} \frac{\Delta n_j}{\Delta n_j^{(\text{SO})}} J_{ij}^{(\text{SO})}, \quad (28)$$

where $\Delta n_i^{(\text{SO})}$ and $\Delta n_i^{(\text{SOS})}$ are the spin population at site i calculated using the NO basis and SO basis, respectively, and $J_{ij}^{(\text{SO})}$ is the J_{ij} value calculated with the SO scheme. This spin population scaling is based on the assumption that the J_{ij} values are proportional to the spin populations at sites i and j for small deviations. We call this scheme as single-site orthogonalization with spin population scaling (SOS). The calculated J_{ij} as functions of r_{ij} based on the SOS scheme are shown in Fig. 5(c). We can see that the J_{ij} profiles converge well and are almost independent of the choice of basis sets for large number of orbitals.

We also calculated the Curie temperature T_C from the J_{ij} values. Within the mean field approximation, the

Curie temperature T_C can be obtained as the maximum eigenvalue of the matrix Θ with the matrix elements

$$[\Theta]_{ij} = \frac{2}{3k_B} \times \begin{cases} \sum_{\mathbf{R} \neq \mathbf{0}} J_{\mathbf{0}i, \mathbf{R}i}, & i = j \\ \sum_{\mathbf{R}} J_{\mathbf{0}i, \mathbf{R}j}, & i \neq j \end{cases} \quad (29)$$

where $J_{\mathbf{0}i, \mathbf{R}j}$ is the exchange coupling constant between site i at cell $\mathbf{0}$ and site j at cell \mathbf{R} . The summation in Eq. (29) was derived by subtracting the self-interaction term from the periodic sum as described in Ref. [42]. The calculated T_C for different basis sets are shown in Fig. 6. As expected from the J_{ij} profiles, the T_C calculated with the SOS scheme shows convergent behavior as N_b increases and converges at a value about a few tens of percent higher than the experimental value, while that derived from the SO scheme gradually decreases with increasing N_b . In contrast, the T_C s calculated from the NO and LO schemes show large deviations at large N_b . These results show that the NO and LO schemes are unsuitable for the Liechtenstein calculation within the LCAO approximation, and that the SOS scheme is the most stable scheme for calculating T_C among the schemes examined.

B. Curie temperatures of hcp Co and fcc Ni

In addition to bcc Fe, we calculated J_{ij} and T_C of hcp Co and fcc Ni for different orthogonalization schemes and different choices of basis sets. Figure 7 shows the calculated Curie temperatures of hcp Co and fcc Ni. It can be seen in Fig. 7 that the Curie temperatures derived from the SOS scheme show convergent behavior while those derived from the SO scheme gradually decrease. The results for the NO and LO schemes show unstable behavior except for the LO results for fcc Ni. These results are another evidence for the SOS scheme being the most stable scheme for the Liechtenstein calculation.

C. J_{ij} profiles for dhcp Nd and rhombohedral Sm

Next, we calculated J_{ij} for dhcp Nd and rhombohedral Sm with different orthogonalization schemes and choices of basis sets. Figure 8(a)-(b) shows the calculated J_{ij} as functions of atomic distance r_{ij} for the NO scheme, and Figure 8(c)-(d) for the SOS scheme. It can be seen in Figure 8(a) and (b) that the calculated J_{ij} values by the NO scheme vary more drastically with the basis sets than those of transition metals in the previous section, and that it is almost impossible to determine the correct results from the NO calculations. In contrast, the J_{ij} values from the SOS scheme converge slowly with increasing basis set size, as can be seen in Fig. 8(c) and (d). Moreover, small negative J_{ij} values for long ranges are obtained for both cases in the SOS calculations. These results agree with experimental reports on Nd and Sm exhibiting spiral and complicated magnetic orders [47], which are attributed to antiferromagnetic exchange interactions.

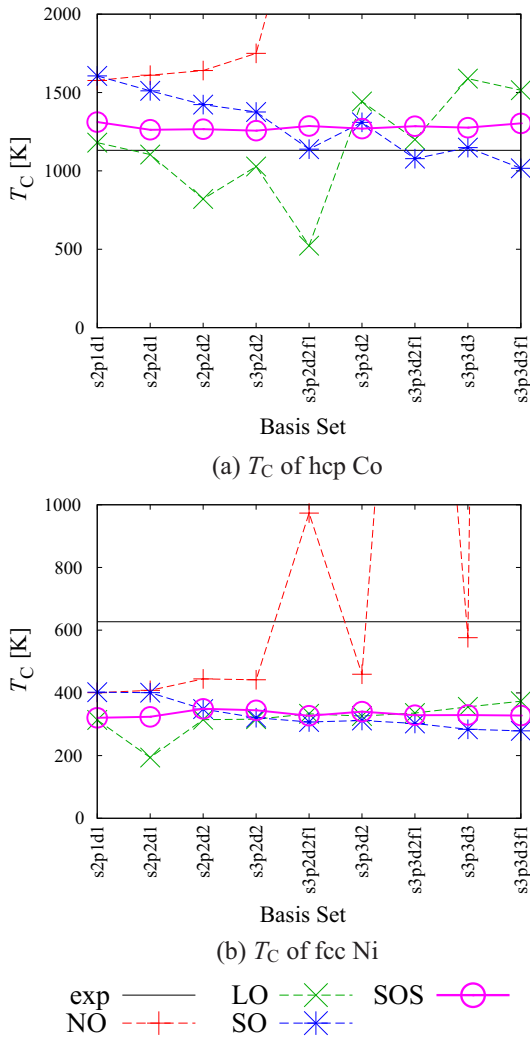


FIG. 7. Calculated Curie temperatures of transition metals within mean field approximation for different orthogonalization schemes and different choices of basis sets, together with the experimental values. (Color online)

V. SUMMARY

We introduced a new orthogonalization scheme called single-site orthogonalization (SO) for calculating exchange coupling constants J_{ij} within the LCAO approximation, and compared the calculated J_{ij} for bcc Fe, hcp Co, fcc Ni, dhcp Nd and rhombohedral Sm by the SO scheme with those calculated by the non-orthogonal (NO) and Löwdin orthogonalization (LO) schemes. We found that the SO scheme underestimates J_{ij} slightly as the number of basis functions N_b increases, whereas the NO and LO schemes give strongly fluctuating results for large N_b . The underestimation by the SO scheme can be well corrected by introducing spin-population scaling, which we call single-site orthogonalization with spin population scaling (SOS). Using the SOS scheme, we successfully obtained converged Curie temperatures for transition metals and small negative J_{ij} values for rare earth metals. We believe that the formalism introduced in this study opens up new prospects for understanding the co-existence of localized and itinerant electrons.

ACKNOWLEDGMENTS

The authors thank Hisazumi Akai and Munehisa Matsumoto for fruitful discussions and valuable comments.

This work was supported in part by MEXT, Japan as Program for Promoting Researches on the Supercomputer Fugaku, DPMSD, the Elements Strategy Initiative Project (ESICMM, Grant No. JPMXP0112101004) under the auspices of MEXT, as well as KAKENHI Grant No. 17K04978. Some of the calculations were performed using the supercomputers at ISSP, The University of Tokyo, and Tsubame, Tokyo Institute of Technology, as well as the K computer, RIKEN Project Nos. hp180206, and hp190169.

- [1] S. Sugimoto, J. Phys. D: Appl. Phys. **44**, 064001 (2011).
- [2] K. Hono and H. Sepehri-Amin, Scripta Mater. **67**, 530–535 (2012).
- [3] S. Hirose, M. Nishino, and S. Miyashita, Adv. Nat. Sci: Nanosci. Nanotechnol **8**, 013002 (2017).
- [4] S. Li, B. Gu, H. Bi, Z. Tian, G. Xie, Y. Zhu, and Y. Du, J. Appl. Phys. **92**, 7514–7518 (2002).
- [5] W. F. Li, T. Ohkubo, and K. Hono, Acta Mater. **57**, 1337–1346 (2009).
- [6] T.-H. Kim, S.-R. Lee, S. Namkuma, and T.-S. Jang, J. Alloys Compd. **537**, 261–268 (2012).
- [7] H. Sepehri-Amin, T. Ohkubo, T. Shima, and K. Hono, Acta Mater. **60**, 819–830 (2012).
- [8] U. M. R. Seelam, L. Liu, T. Akiya, H. Sepehri-Amin, T. Ohkubo, N. Sakuma, M. Yano, A. Kato, and K. Hono, J. Magn. Magn. Mater. **412**, 234–242 (2016).
- [9] T. T. Sasaki, T. Ohkubo, and K. Hono, Acta Mater. **115**, 269–277 (2016).
- [10] X. D. Xu, T. T. Sasaki, J. N. Li, Z. J. Dong, H. Sepehri-Amin, T. H. Kim, T. Ohkubo, T. Schrefl, and K. Hono, Acta Mater. **156**, 146–157 (2018).
- [11] T. Fukushima, H. Shinya, H. Fujii, K. Sato, H. Katayama-Yoshida, and P. H. Dederichs, J. Phys.: Condens. Matter, **27**, 015501 (2015).
- [12] B. Balasubramanian, P. Manchanda, R. Skomski, P. Mukherjee, S. R. Valloppilly, B. Das, G. C. Hadjipanayis, and D. J. Sellmyer, Appl. Phys. Lett. **108**, 152406 (2016).
- [13] A. Saengdeejing, Y. Chen, M. Matsuura, and S. Sugimoto, Journal of the Chinese Chemical Society **63**, 506–512 (2016).
- [14] Y. Tatetsu, S. Tsuneyuki, and Y. Gohda, Phys. Rev. Applied **6**, 064029, (2016).

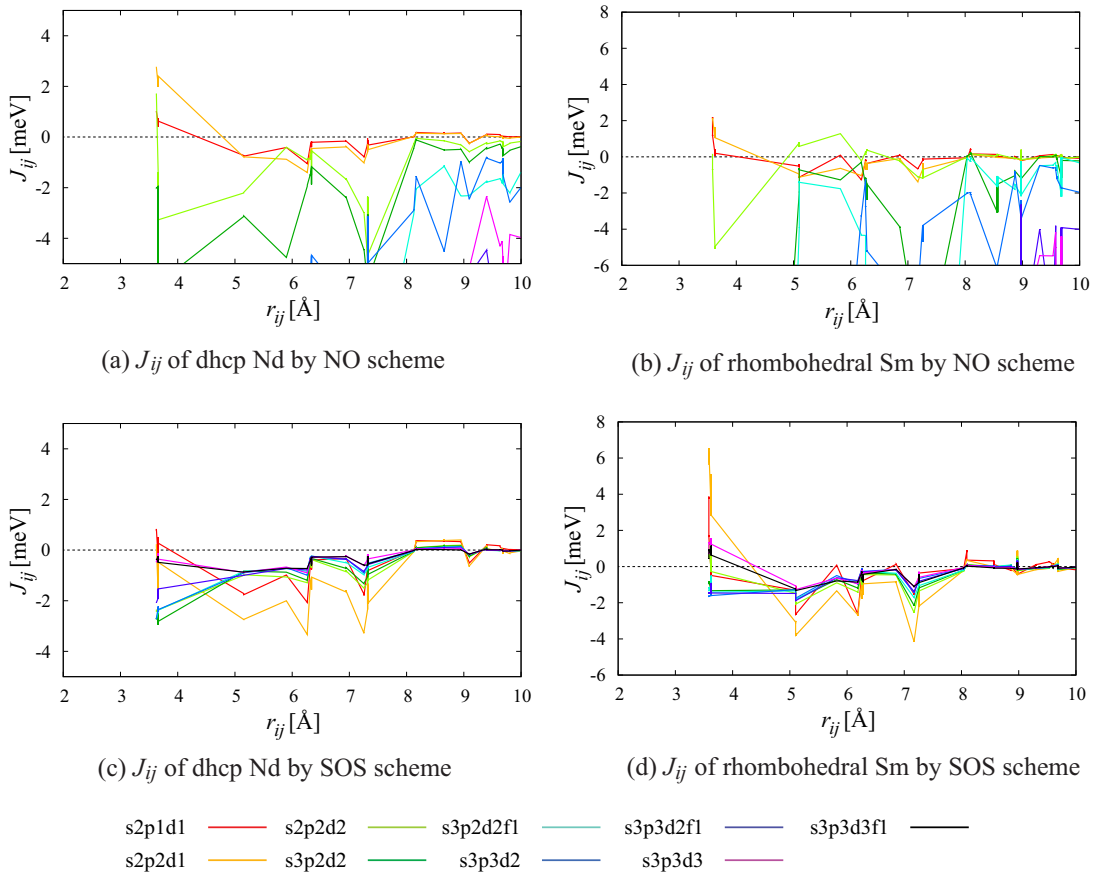


FIG. 8. Exchange coupling constants J_{ij} of (a) and (b) dhcp Nd and (c) and (d) rhombohedral Sm as functions of atomic distances r_{ij} calculated by the SOS scheme and different choices of basis sets. (Color online)

- [15] Z. Torbatian, T. Ozaki, S. Tsuneyuki, and Y. Gohda, Appl. Phys. Lett. **104**, 242403 (2014).
- [16] N. Umetsu, A. Sakuma, and Y. Toga, Phys. Rev. B **93**, 014408 (2016).
- [17] T. Fukazawa, H. Akai, Y. Harashima, and T. Miyake, J. Appl. Phys. **122** 053901 (2017).
- [18] H. Akai, Scripta Materialia **154**, 300–304 (2018).
- [19] Y. Gohda, Y. Tatetsu, and S. Tsuneyuki, Mater. Trans. **59**, 332–337 (2018).
- [20] C. E. Patrick and J. B. Staunton, Phys. Rev. B **97**, 224415 (2018).
- [21] Y. Tatetsu, S. Tsuneyuki, and Y. Gohda, Materialia **4**, 388–394 (2018).
- [22] T. Fukazawa, H. Akai, Y. Harashima, and T. Miyake, IEEE Trns. Magn. **55**, 2895669 (2019).
- [23] C. E. Patrick, M. Matsumoto, and J. B. Staunton, J. Magn. Magn. Mater. **477**, 147–155 (2019).
- [24] A. M. Schönhöbel R. Madugundo, O. Yu. Vekilova, O. Eriksson, H. C. Herper, J. M. Barandiarán, and G. C. Hadjipanayis. Journal of Alloys and Compounds **786**, 969–974 (2019).
- [25] A. L. Tedstone, C. E. Patrick, S. Kumar, R. S. Edwards, M. R. Lees, G. Balakrishnan, and J. B. Staunton, Phys. Rev. Materials **3**, 034409 (2019).
- [26] T Oguchi, Kiyoyuki Terakura and Noriaki Hamada, J. Phys. F: Met. Phys. **13**, 145 (1983).
- [27] A. I. Liechtenstein, M. I. Katsnelson, V. P. Antropov, and V. A. Gubanov, J. Magn. Magn. Mater. **67**, 65–74 (1987).
- [28] H. Shiba, Prog. Theor. Phys. **46**, 77 (1971)
- [29] H. Akai, Physica **86-88B**, 539 (1977).
- [30] H. Akai, J. Phys. Soc. Japan **51**, 468 (1982).
- [31] S. Lounis, P. Mavropoulos, P. H. Dederichs, and S. Blügel, Phys. Rev. B, **72**, 224437, (2005).
- [32] H. Ebert, D. Ködderitzsch, and J. Minár, Rep. Prog. Phys. **74**, 096501 (2011).
- [33] D. S. G. Bauer, Doctoral dissertation, RWTH Aachen University (2013).
- [34] S. Frota-Pessôa, R. B. Muniz, and J. Kudrnovský, Phys. Rev. B **62**, 5293–5296 (2000).
- [35] M. Pajda, J. Kudrnovský, I. Turek, V. Drchal, and P. Bruno, Phys. Rev. B **64**, 174402 (2001).
- [36] I. Turek, J. Kudrnovský, G. Bihlmayer, and S. Blügel, J. Phys.: Condens. Matter **15**, 2771 (2003).
- [37] H. Wang, P.-W. Ma, and C. H. Woo, Phys. Rev. B **82**, 144304, (2010).
- [38] Y. O. Kvashnin, O. Grånäs, I. Di Marco, M. I. Katsnelson, A. I. Lichtenstein, and O. Eriksson, Phys. Rev. B **91**, 125133, (2015).
- [39] A. Szilva, D. Thonig, P. F. Bessarab, Y. O. Kvashnin, D. C. M. Rodrigues, R. Cardias, M. Pereiro, L. Nordström, A. Bergman, A. B. Klautau, and O. Eriksson, Phys. Rev. B **96**, 144413 (2017).

- [40] M. J. Han, T. Ozaki, and J. Yu, Phys. Rev. B **70**, 184421 (2004).
- [41] H. Yoon, T. J. Kim, J.-H. Sim, S. W. Jang, T. Ozaki, and M. J. Han, Phys. Rev. B **97**, 125132 (2018).
- [42] A. Terasawa, M. Matsumoto, T. Ozaki, and Y. Gohda, J. Phys. Soc. Jpn. **88** 114706 (2019).
- [43] T. Ozaki, Phys. Rev. B **67**, 155108 (2003).
- [44] J. P. Perdew, K. Burke, and M. Ernzerhof, Phys. Rev. Lett. **77**, 3865–3868 (1996).
- [45] T. Ozaki, Phys. Rev. B **75**, 035123 (2007).
- [46] I. Morrison, D. M. Bylander, and L. Kleinman, Phys. Rev. B **47**, 6728 (1993).
- [47] J. M. D. Coey, *Magnetism and magnetic materials* (Cambridge University Press, Cambridge, 2010).